$\mathcal{PT}$-symmetry-induced evolution of sharp asymmetric line shapes and high-sensitivity refractive index sensors in a three-cavity array

Jiahua Li,[1,*] Rong Yu,[2] Chunling Ding,[3] and Ying Wu[4,†]

[1]*School of Physics, MOE Key Laboratory of Fundamental Physical Quantities Measurement, Huazhong University of Science and Technology, Wuhan 430074, People's Republic of China*

[2]*School of Science, Hubei Province Key Laboratory of Intelligent Robot, Wuhan Institute of Technology, Wuhan 430073, People's Republic of China*

[3]*School of Physics and Electronics, Henan University, Kaifeng 475004, People's Republic of China*

[4]*Wuhan National Laboratory for Optoelectronics and School of Physics, Huazhong University of Science and Technology, Wuhan 430074, People's Republic of China*

(Received 17 November 2015; published 8 February 2016)

It is important to control and tune the Fano-resonance spectra to achieve a large slope with, in addition, a relatively high extinction ratio for low-power optical switching and high-sensitivity sensing. Here, we explore the evolution of sharp asymmetric Fano-like line shapes in a three-cavity array with local parity-time ($\mathcal{PT}$) symmetry. In this three-cavity configuration, a single cavity is coupled to a $\mathcal{PT}$-symmetric combination of two cavities via a common waveguide. The influences of local $\mathcal{PT}$ symmetry on the asymmetric Fano-like line shapes are investigated by monitoring the output transmission spectra at various system parameters. It is found that both the slope and the extinction ratio within the sharp asymmetric line shapes can be significantly enhanced by introducing the $\mathcal{PT}$-symmetric unit, compared with the configuration of two indirectly coupled cavities. Subsequently we discuss the application of such a $\mathcal{PT}$-assisted configuration as a family of high-sensitivity refractive index sensors by numerical analysis. For practical parameters based on microring resonators, the best sensitivity of refractive index sensors is more than five orders of magnitude larger than two indirectly coupled lossy cavities. The proposed scheme can be implemented in current state-of-the-art experiments. This investigation can help us to understand the interplay between the Fano resonance and $\mathcal{PT}$ symmetry.

DOI: 10.1103/PhysRevA.93.023814

I. INTRODUCTION

Optical cavities with high-quality factors and small mode volumes [1] have witnessed rapid progress in recent years and have been implemented in many systems as a key functional building block for buffering, modulating, filtering, switching, and sensing [2–8], just to name a few examples. The basic geometry, consisting of a channel waveguide side coupled with a single-mode cavity, as shown in Fig. 1(a), has been studied theoretically and experimentally based on the scattering theory [9], temporal coupled-mode theory [10], and quantum-optics approach [11]. Theoretically, the resonance line shape of such a conventional single cavity is symmetrical with respect to its resonance wavelengths [9–12]. However, when the coupling of two single-mode cavities (or several single-mode cavities) to a channel waveguide exists in a system, as described in Fig. 1(b), the transmission characteristics can be dramatically modified in the spectra [13]. Generally speaking, coupled-cavity structures can be categorized into two typical geometries: (i) directly coupled cavities (cavity-cavity) [14–18] and (ii) indirectly coupled cavities via a common waveguide (cavity-waveguide-cavity) [19–30]. For both direct and indirect coupling structures, different characteristics in the output transmission spectra, such as mode splitting [13], electromagnetically induced transparency–like transmission [14,15,21,24], and Fano-type resonances [28–30], have been revealed and observed from different views. In particular, the generated asymmetric Fano-resonance line shapes have been proposed to enhance the slope sensitivity [29], compared with that of a conventional single cavity [6]. Accordingly, for a practical application, coupled-cavity structures are often used to design highly sensitive sensors by measuring the output intensity change from the cavity at a fixed wavelength [29–31].

In the past decade, there has been great interest in discrete and continuous systems that are symmetric under parity-time ($\mathcal{PT}$) reversal. Originally, $\mathcal{PT}$-symmetric notions have been proposed within the context of mathematical physics [32–35]. Recently, $\mathcal{PT}$-symmetric ideas have been introduced within the framework of optics [36–52] by delicately manipulating the amount of gain and loss in the considered settings. It is recognized that $\mathcal{PT}$-symmetric systems undergo an abrupt phase transition when the gain-to-loss ratio is properly varied [39,41]. Below a certain gain-to-loss ratio threshold value, the system is in the unbroken $\mathcal{PT}$-symmetric phase and has purely real eigenvalues. On the other hand, above this gain-to-loss ratio threshold value, the system is in the broken $\mathcal{PT}$-symmetric phase. In this broken-$\mathcal{PT}$ phase, a pair of supermode possesses effective indices that are a pair of complex conjugate eigenvalues, such that one mode experiences gain and the other loss. The threshold value mentioned above, where two real eigenvalues merge and become complex, is called an exceptional point (EP; it is a typical accompaniment of $\mathcal{PT}$-symmetric systems), marking an obvious boundary between different optical properties. The optical devices based on the constructed $\mathcal{PT}$-symmetric structures could provide a great potential for future applications in on-chip integrated optics [53–66].

*huajia_li@163.com
†yingwu2@126.com

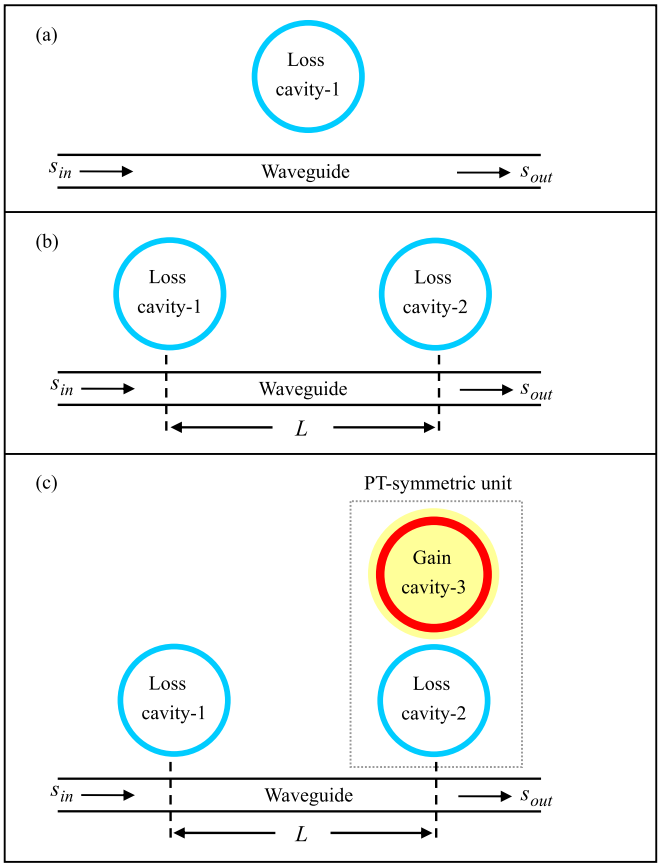

FIG. 1. (a) Schematic of a single-mode loss cavity (denoted 1) side coupled to a channel waveguide. s_{in} and s_{out} denote the amplitudes of the electromagnetic waves incident from the left side and leaving from the right side of the waveguide, respectively. (b) Schematic of two single-mode loss cavities (denoted 1 and 2) side coupled to a common waveguide. The two cavities are separated by a distance L much longer than the wavelength so that there is no direct coupling between the two cavities. (c) Schematic of the $\mathcal{PT}$-assisted three-cavity array (denoted 1, 2, and 3) derived by introducing an auxiliary single-mode gain cavity in (b). The gain cavity, 3, balances the loss of cavity 2. Such coupled dimer structures with balanced gain and loss are referred to as having $\mathcal{PT}$ symmetry [47–51].

Inspired by the advances [19,21,24,27,28] and $\mathcal{PT}$ concepts [47–51] in coupled-cavity structures, the inclusion of a $\mathcal{PT}$-symmetrical unit with balanced gain and loss [see Fig. 1(c)] can greatly enhance the asymmetric line shapes of the Fano resonance in our proposed three-cavity array, which gives rise to changes in the output transmission that are faster than the changes from the previous mode [see Fig. 1(b)]. Subsequently we discuss its application as a refractive index (RI) sensor. With the output transmission at a fixed wavelength that changes much more rapidly than it does in two indirectly coupled cavities without the assistance of a $\mathcal{PT}$-symmetrical unit, the results shows that the enhanced sensitivity of the present device to changes in the RI can be achieved efficiently. This work may open a new avenue for line-shape engineering of Fano resonances in photonic structures based on $\mathcal{PT}$ symmetry.

The remainder of the paper is organized in the following way. In Sec. II, we introduce the theoretical model and give the coupled-mode equations for the evolution of the cavity modes. In Sec. III, we investigate in detail the optical transmission characteristics of three possible configurations: (i) a single cavity, (ii) two indirectly coupled cavities, and (iii) a $\mathcal{PT}$-assisted three-cavity array (also see Fig. 1). In Sec. IV, we demonstrate the application of such a $\mathcal{PT}$-assisted three-cavity array as a class of high-sensitivity RI sensor by numerical analysis. Finally, in Sec. V, we summarize our results.

II. THEORETICAL MODEL, COUPLED-MODE EQUATIONS, AND SOLUTIONS

We consider a class of three-cavity array as shown in Fig. 1(c). In the three-cavity configuration, two single-mode cavities (denoted 1 and 2) are loss and the other (denoted 3) is gain. Because cavity 1 and cavity 2 are separated by a distance L much longer than the wavelength, there is no direct modal overlap (i.e., no coupling) between the cavity modes, but nevertheless, the two cavities are coupled strongly through a common waveguide. As shown in Refs. [10,11,27,30], this indirect interaction parameter g_{eff} (defined later) is dependent on the cavity-waveguide coupling strength (κ_{1e}, κ_{2e}) and the propagating phase factor [$\theta = \beta(\omega)L$, where $\beta(\omega)$ is the waveguide dispersion relationship]. An experimental implementation of two indirectly coupled cavities via the waveguide (i.e., cavity-waveguide-cavity) has been realized in Refs. [19,21,24,27,28]. Additionally, the loss cavity 2 and the gain cavity 3 have direct coupling to the strength J, which is dictated by the mutual overlap of their respective modal fields throughout the interaction region and is tuned by their separation [47–51]. Thus these two directly coupled cavities can form a $\mathcal{PT}$-symmetrical arrangement of our structure. A realization of $\mathcal{PT}$-symmetric coupled cavities has also been demonstrated experimentally in Refs. [47–51].

We denote the amplitudes c_j for each cavity j ($j = 1, 2, 3$). The amplitudes of the incoming and outgoing fields in the waveguide are represented by s_{in} and s_{out}, respectively. The squared magnitudes of these amplitudes are equal to the powers in the modes. The characteristic equations for the temporal evolution of the cavity modes together with the input-output relation are yielded by [10,11,27,30]

$$\frac{dc_1}{dt} = -\left(i\omega_1 + \frac{\kappa_{1i}}{2} + \frac{\kappa_{1e}}{2}\right)c_1 - g_{\text{eff}}c_2 - \sqrt{\frac{\kappa_{1e}}{2}}s_{\text{in}}, \quad (1)$$

$$\frac{dc_2}{dt} = -\left(i\omega_2 + \frac{\kappa_{2i}}{2} + \frac{\kappa_{2e}}{2}\right)c_2 - g_{\text{eff}}c_1 - iJc_3 - e^{i\theta}\sqrt{\frac{\kappa_{2e}}{2}}s_{\text{in}}, \quad (2)$$

$$\frac{dc_3}{dt} = -\left(i\omega_3 + \frac{\kappa_3}{2}\right)c_3 - iJc_2, \quad (3)$$

$$s_{\text{out}} = e^{i\theta}\left(s_{\text{in}} + \sqrt{\frac{\kappa_{1e}}{2}}c_1\right) + \sqrt{\frac{\kappa_{2e}}{2}}c_2, \quad (4)$$

where ω_j is the resonance frequency of each cavity mode c_j ($j = 1, 2, 3$). κ_{1i} (κ_{2i}) and κ_{1e} (κ_{2e}), respectively, are the intrinsic loss rate and the external coupling loss rate of cavity 1 (cavity 2). The total cavity 1 (cavity 2) loss rate is $\kappa_1 = \kappa_{1i} + \kappa_{1e}$ ($\kappa_2 = \kappa_{2i} + \kappa_{2e}$). In cavity 3, the effective loss rate $\kappa_3 = \kappa_{3i} + \kappa_{3e} - \xi$ is reduced by the pump gain ξ

(round-trip energy gain) [47–51]. Whether $\kappa_3 > 0$ (loss) or $\kappa_3 < 0$ (gain) depends on ξ. Here, we assume that $\kappa_3 < 0$ corresponds to an active gain cavity. From Eqs. (1) and (2), it is easy to find that an indirect interaction between loss cavity 1 and loss cavity 2 exists, with the effective coupling strength $g_{\rm eff} = \frac{1}{2}e^{i\theta}\sqrt{\kappa_{1e}\kappa_{2e}}$ [27,28,67,68]. From this expression, it is evident that $g_{\rm eff}$ is closely related to the propagating phase factor θ and the cavity-waveguide coupling loss rates κ_{1e} and κ_{2e}. Experimentally, the parameters κ_{1e} and κ_{2e} can be continuously adjusted by tuning the waveguide-cavity gap. In particular, the propagating phase factor $\theta = \beta(\omega)L$, where $\beta(\omega)$ is the waveguide's dispersion and L denotes the waveguide's distance between the coupling regions of the two cavities, plays an important role in the analysis of the transmission properties of our $\mathcal{PT}$-assisted three-cavity array. The parameter θ is fully controllable by adjusting the length of the waveguide between the cavities. In photonic crystal systems, this length L can be adjusted by changing the number of periods [69]. Note that the phase θ is invariant with the period 2π. On the other hand, the dispersion $\beta(\omega)$ of the waveguide can also be used to control the propagating phase factor θ. In Eqs. (1)–(3), we ignore the saturation effect and restrict ourselves to small-signal analysis.

We work in the frequency domain of the $\mathcal{PT}$-assisted three-cavity system and set $dc_j/dt = -i\omega c_j$ when the electromagnetic wave at a frequency ω is launched into the system, so from Eqs. (1)–(3) we can obtain

$$\frac{c_1}{s_{\rm in}} = \frac{e^{i\theta}\sqrt{\kappa_{2e}/2}g_{\rm eff} + \sqrt{\kappa_{1e}/2}(i\Delta_2 - \kappa_2/2 + \Omega)}{(i\Delta_1 - \kappa_1/2)(i\Delta_2 - \kappa_2/2 + \Omega) - g_{\rm eff}^2}, \quad (5)$$

$$\frac{c_2}{s_{\rm in}} = \frac{\sqrt{\kappa_{1e}/2}g_{\rm eff} + e^{i\theta}\sqrt{\kappa_{2e}/2}(i\Delta_1 - \kappa_1/2)}{(i\Delta_1 - \kappa_1/2)(i\Delta_2 - \kappa_2/2 + \Omega) - g_{\rm eff}^2}, \quad (6)$$

$$\frac{c_3}{c_2} = \frac{iJ}{i\Delta_3 - \kappa_3/2}, \quad (7)$$

where we have defined $\Omega = J^2/(i\Delta_3 - \kappa_3/2)$, $\Delta_1 = \omega - \omega_1$, $\Delta_2 = \omega - \omega_2$, and $\Delta_3 = \omega - \omega_3$, respectively. Plugging Eqs. (5) and (6) into Eq. (4), the amplitude transmission is readily derived as

$$t(\omega) \equiv \frac{s_{\rm out}}{s_{\rm in}} = e^{i\theta}\left(1 + \sqrt{\frac{\kappa_{1e}}{2}}\frac{c_1}{s_{\rm in}}\right) + \sqrt{\frac{\kappa_{2e}}{2}}\frac{c_2}{s_{\rm in}}, \quad (8)$$

where two coefficients, $c_1/s_{\rm in}$ and $c_2/s_{\rm in}$, are given by the above analytical expressions (5) and (6), respectively. Finally, the power transmission of the coupled system in Fig. 1(c) is written as

$$T(\omega) = |t(\omega)|^2. \quad (9)$$

Before proceeding, it is worth pointing out that (i) when $J = g_{\rm eff} = 0$, we can obtain the results for a single cavity in Fig. 1(a); and (ii) when $J = 0$, we can also arrive at the results of two indirectly coupled lossy cavities without the assistance of a $\mathcal{PT}$ structure in Fig. 1(b). $\mathcal{PT}$ symmetry requires the conditions that $\omega_3 = \omega_2$ and $\kappa_3 = -\kappa_2$ [47–51]. In view of this, in the following discussion we assume that the three cavities have the degenerate resonance frequencies $\omega_1 = \omega_2 = \omega_3 = \omega_0$, which thus lead to the same detunings $\Delta_1 = \Delta_2 = \Delta_3 = \Delta$.

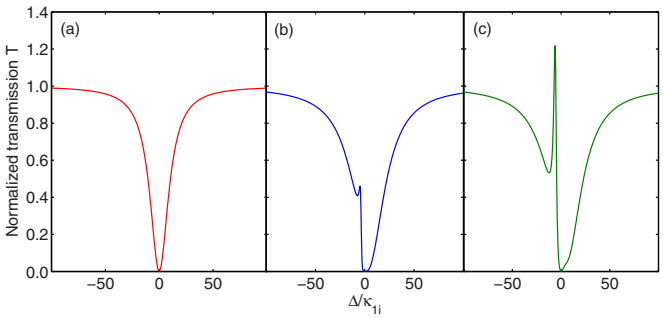

FIG. 2. (a) Power transmission spectrum of a single cavity as shown in Fig. 1(a). System parameters are chosen as $\kappa_{1e} = 20\kappa_{1i}$. (b) Power transmission spectrum of the two indirectly coupled cavities in Fig. 1(b). Here the two cavities are identical. System parameters are chosen as $\kappa_{2e} = \kappa_{1e} = 20\kappa_{1i}$, $\kappa_{2i} = \kappa_{1i}$, and $\theta = \pi/8$, respectively. (c) Power transmission spectrum of the $\mathcal{PT}$-assisted three-cavity array in Fig. 1(c). System parameters are chosen as $\kappa_{2e} = \kappa_{1e} = 20\kappa_{1i}$, $\kappa_{2i} = \kappa_{1i}$, $\theta = \pi/8$, $J = 8\kappa_{1i}$, and $\kappa_3 = -21\kappa_{1i}$, respectively.

III. OPTICAL TRANSMISSION FEATURES OF DIFFERENT WAVEGUIDE-CAVITY STRUCTURES

The output transmission spectra can be calculated using Eqs. (5)–(9) for three possible configurations (a single cavity, two indirectly coupled cavities, and a $\mathcal{PT}$-assisted three-cavity array). In Fig. 2, we plot the power transmission spectra $T(\Delta)$ of the cavity system as a function of the detuning Δ/κ_{1i}. For a side-coupled lossy cavity as shown in Fig. 1(a), the power transmission can be expressed in the form

$$T(\Delta) = \frac{4\Delta^2 + \kappa_{1i}^2}{4\Delta^2 + (\kappa_{1i} + \kappa_{1e})^2}, \quad (10)$$

which has the form of a single Lorentzian-shaped dip with width κ_{1e}. For clarity, we also display its corresponding curve in Fig. 2(a). It is shown in Fig. 2(a) that for the case of a single cavity, the transmission spectrum does exhibit a symmetric Lorentzian line shape with respect to the resonance frequency $\Delta = 0$ at which the transmission falls to $T(\Delta = 0) = 0$.

For two indirectly coupled lossy cavities via a common waveguide, in Fig. 1(b), the corresponding power transmission is determined as

$$T(\Delta,\theta) = \frac{\left(4\Delta^2 + \kappa_i^2\right)^2}{\mathcal{D}_-(\Delta,\theta)\mathcal{D}_+(\Delta,\theta)}, \quad (11)$$

where we have defined $\mathcal{D}_-(\Delta,\theta) = (2\Delta - \kappa_e\sin\theta)^2 + (\kappa + \kappa_e\cos\theta)^2$ and $\mathcal{D}_+(\Delta,\theta) = (2\Delta + \kappa_e\sin\theta)^2 + (\kappa - \kappa_e\cos\theta)^2$, respectively. In the above derivation, we have supposed that both cavities have the same dissipations for facilitating the discussion, namely, $\kappa_{1i} = \kappa_{2i} = \kappa_i$, $\kappa_{1e} = \kappa_{2e} = \kappa_e$, and $\kappa_1 = \kappa_2 = \kappa$. As can be seen from Eq. (11), the added second loss cavity, which constitutes the cavity-waveguide-cavity structure, introduces the backward propagating lights that can perturb the phase of the light transmitted and hence result in complex constructive and destructive interference. For example, when $\theta = n\pi$, with n being an integral number, the two resonances are degenerate. In this case, the corresponding power transmission spectrum is manifested as a symmetric Lorentzian line shape with width $2\kappa_e$, given

by $T = \frac{4\Delta^2+\kappa_i^2}{4\Delta^2+(\kappa_i+2\kappa_e)^2}$. However, when $\theta = n\pi + \pi/8$, the Fano-like resonance line shape is produced by involving interference [30]. Consequently, it is shown in Fig. 2(b) that the transmission spectrum of two indirectly coupled cavities becomes asymmetric due to such interference when the propagating phase factor θ is chosen properly.

For the $\mathcal{PT}$-assisted three-cavity array in Fig. 1(c), the resulting power transmission is given by

$$T(\Delta,\theta) = \frac{\left(4\Delta^2+\kappa_i^2\right)\left[4\Delta^2\kappa_e^2+(4J^2-4\Delta^2-\kappa\kappa_i)^2\right]}{\mathcal{D}_{\mathcal{PT}}(\Delta,\theta)}, \tag{12}$$

where we have defined $\mathcal{D}_{\mathcal{PT}}(\Delta,\theta)=[2\Delta(4J^2-4\Delta^2-\kappa^2)-\kappa_e^2(2\Delta\cos 2\theta+\kappa\sin 2\theta)]^2+[\kappa(4J^2-4\Delta^2-\kappa^2)+\kappa_e^2(\kappa\cos 2\theta-2\Delta\sin 2\theta)]^2$. Similarly, the cavity system parameters have been chosen as $\kappa_{1i}=\kappa_{2i}=\kappa_i$, $\kappa_{1e}=\kappa_{2e}=\kappa_e$, $\kappa_1=\kappa_2=\kappa$, and $\kappa_3=-\kappa$ for $\mathcal{PT}$ case. It also follows from $\mathcal{D}_{\mathcal{PT}}(\Delta,\theta)$ that the change of the line shapes is periodic, with a periodicity of π. Compared with two indirectly coupled lossy cavities, the $\mathcal{PT}$-assisted three-cavity system can achieve a sharper and higher extinction ratio asymmetric line shape, referred to as Fano-like resonance in Fig. 2(c). Physically, this is because optical $\mathcal{PT}$ symmetry balances the loss of cavity 2. This gain-loss balance of the $\mathcal{PT}$-symmetric structure causes rapid changes in the power transmission in the very narrow frequency ranges, and cavity 3, with gain in the $\mathcal{PT}$-symmetric structure, which works as a dynamical amplifier [65], enhances the transmission peak of Fano resonance at $\Delta = 0$.

According to Eqs. (11) and (12), the line shape of the Fano-like resonance transmission can be changed by varying the propagating phase factor θ. Figure 3 shows the calculated power transmission spectra for nine values of the propagating phase factor θ. As we adjust the waveguide distance L between the coupling regions of the two loss cavities, increasing θ from 0 to π, it is shown in these figures that the transmission line changes from a symmetrical to an asymmetrical line shape. Note that the power transmission spectra at $\theta = C_1$ (C_1 is an arbitrary angle from 0 to π) and $\theta = \pi - C_1$ are horizontal mirror symmetric as shown in Fig. 3. The above-mentioned mirror-symmetric phenomenon can be well explained in terms of the previous relationships $\mathcal{D}_-(\Delta,\theta=C_1)\mathcal{D}_+(\Delta,\theta=C_1)=\mathcal{D}_-(-\Delta,\theta=\pi-C_1)\mathcal{D}_+(-\Delta,\theta=\pi-C_1)$ in Eq. (11) for Fig. 3(a) and $\mathcal{D}_{\mathcal{PT}}(\Delta,\theta=C_1)=\mathcal{D}_{\mathcal{PT}}(-\Delta,\theta=\pi-C_1)$ in Eq. (12) for Fig. 3(b), respectively. Obviously, the Fano-resonance line shapes can be controlled by tuning the value of θ. On the other hand, Fig. 3 also displays the periodicity of the power transmission spectra. The power transmission spectra at $\theta = C_2$ (C_2 is an arbitrary angle from 0 to π) and $\theta = \pi + C_2$ are exactly the same due to the fact that $\mathcal{D}_-(\Delta,\theta=C_2)\mathcal{D}_+(\Delta,\theta=C_2)=\mathcal{D}_-(\Delta,\theta=\pi+C_2)\mathcal{D}_+(\Delta,\theta=\pi+C_2)$ in Eq. (11) for Fig. 3(a) and $\mathcal{D}_{\mathcal{PT}}(\Delta,\theta=C_2)=\mathcal{D}_{\mathcal{PT}}(\Delta,\theta=\pi+C_2)$ in Eq. (12) for Fig. 3(b), respectively. By comparing Fig. 3(a) with Fig. 3(b), it is easy to see that the output spectra of the $\mathcal{PT}$-assisted three-cavity array exhibit a remarkable feature arising from the gain-loss balance and the amplification mechanism [65]; that is, the Fano-resonance line shape becomes sharper and the resonance peak located at $\Delta = 0$ has a higher value than the resonance peak of two indirectly coupled cavities. In brief, a slight spectral shift can give rise to large power variation under the same conditions.

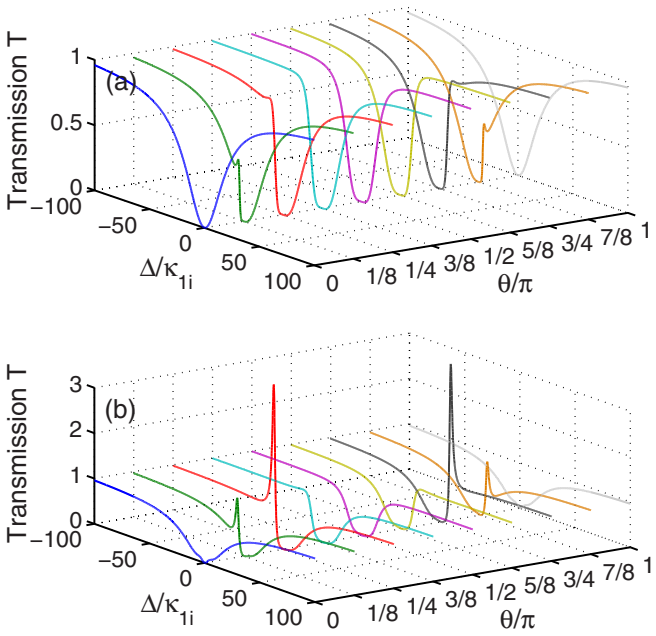

FIG. 3. (a) Representative transmission spectra of the two indirectly coupled cavities in Fig. 1(b) as a function of the detuning Δ/κ_{1i} for nine propagation phase factors θ/π. Other system parameters are chosen as $\kappa_{2e}=\kappa_{1e}=20\kappa_{1i}$ and $\kappa_{2i}=\kappa_{1i}$, respectively. (b) Representative transmission spectra of the $\mathcal{PT}$-assisted three-cavity array in Fig. 1(c) as a function of the detuning Δ/κ_{1i} for nine propagation phase factors θ/π. Other system parameters are chosen as $\kappa_{2e}=\kappa_{1e}=20\kappa_{1i}$, $\kappa_{2i}=\kappa_{1i}$, $J=8\kappa_{1i}$, and $\kappa_3=-21\kappa_{1i}$, respectively.

As is well known, the intercavity coupling strength J between loss cavity 2 and gain cavity 3 is tuned experimentally by changing their distance. In Fig. 4, we display the power transmission characteristics of the $\mathcal{PT}$-assisted three-cavity array by varying the values of J. As can be clearly seen, different asymmetric Fano line shapes are obtained by modulating J in the $\mathcal{PT}$-assisted three-cavity system. Specifically, a sharp peak in the asymmetric line shape increases gradually with increasing J, until a maximum is reached, then it decreases gradually. It is obvious that the sharp asymmetric Fano-resonance line shape is significantly enhanced, as J is in the range of $[5\kappa_{1i},6\kappa_{1i}]$. At the same time, both a large slope and a high extinction ratio can be obtained, which is important for low-power optical switching and high-sensitivity sensing (as discussed in Sec. IV). Note that when $J = 0$, corresponding to the case of two indirectly coupled cavities [see Fig. 1(b)], the transmission peak in the line shape achieves a minimum as shown in Fig. 4.

IV. APPLICATION: HIGH-SENSITIVITY RI SENSORS BASED ON AN ASYMMETRIC TRANSMISSION LINE SHAPE

It has been demonstrated that sharp asymmetric line shapes with a large slope are well suited for application in high-

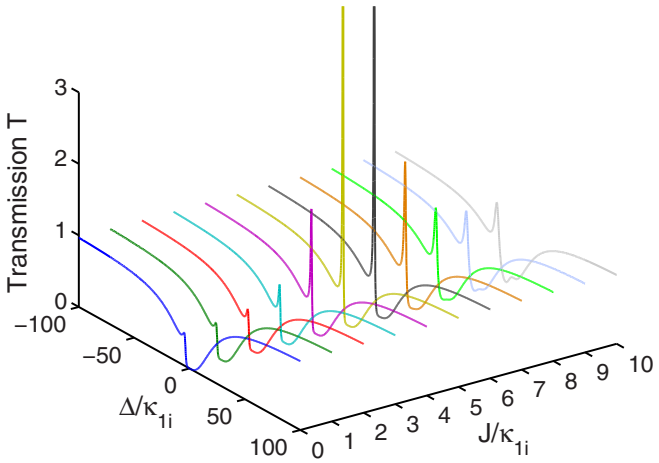

FIG. 4. Representative transmission spectra of the $\mathcal{PT}$-assisted three-cavity array in Fig. 1(c) as a function of the detuning Δ/κ_{1i} for 11 intercavity coupling strengths J/κ_{1i}. Other system parameters are chosen as $\kappa_{2e} = \kappa_{1e} = 20\kappa_{1i}$, $\kappa_{2i} = \kappa_{1i}$, $\theta = \pi/8$, and $\kappa_3 = -21\kappa_{1i}$, respectively.

sensitivity, label-free, microcavity-based biosensing [6,29,70]. Here, the physical mechanism of our proposed sensor is briefly outlined as follows. The working scheme is initially set up by inputting a continuous-wave laser with a fixed wavelength and input power. When the system arrives at the steady state, the change of an environmental parameter, for example, the RI, can alter the optical resonance frequency and then modify the transmission power. As shown in Ref. [29], the resonant wavelength λ for a whispering-gallery mode in a microring resonator with the angular momentum number l is represented by

$$\lambda \simeq 2\pi a[(1-\eta)n_s + \eta n_c]/l, \tag{13}$$

where a is the radius of the microring resonator, η is the fraction of the resonator mode power in the evanescent field, n_s is the RI of the sample surrounding the microring resonator due to the analyte to be detected, and n_c denotes the RI of the microring resonator, respectively. As a result, we can obtain the result

$$\frac{d\lambda}{dn_s} = 2\pi a(1-\eta)/l. \tag{14}$$

Finally, for a given detection wavelength λ, the derivation of the normalized power transmission T can be expressed as

$$\frac{dT}{dn_s} = \frac{dT}{d\lambda}\frac{d\lambda}{dn_s} = -\beta\frac{dT}{d\omega} \propto \frac{dT}{d\omega}, \tag{15}$$

where $\beta = 4\pi^2 ca(1-\eta)/(l\lambda^2)$ is a combined constant, with c being the light speed in free space. The power transmission derivation, $|dT/dn_s|$, defines the detection sensitivity of the $\mathcal{PT}$-assisted three-cavity array. According to Eq. (15), the detection sensitivity is directly proportional to the transmission slope. For convenience, the sensitivity to the RI-induced frequency shift (i.e., the slope of the power transmission curves) is thus introduced by [29,70]

$$S \equiv \left|\frac{dT}{d\omega}\right|. \tag{16}$$

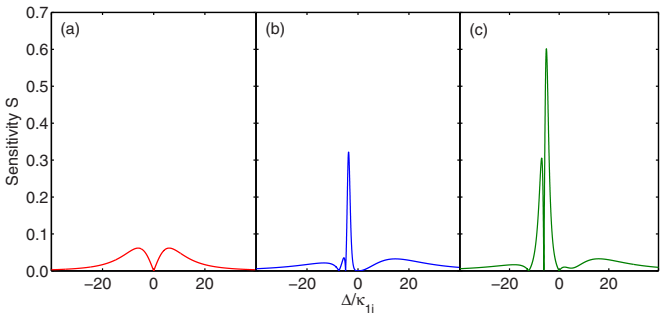

FIG. 5. Sensitivity S (in units of κ_{1i}) as a function of the detuning Δ/κ_{1i} for three configurations: (a) a single cavity, (b) two indirectly coupled cavities, and (c) a $\mathcal{PT}$-assisted three-cavity array. System parameters for the simulation are the same as in Fig. 2.

From Eq. (15), since β is fixed for a given microring resonator, further increase in the sensitivity $|dT/dn_s|$ requires an increase in S, i.e., the transduction rate between the RI-induced frequency shift and the output transmission, which is just the slope of the power transmission spectra. Under practical parameters, $\lambda = 640$ nm, $a = 30$ μm, $l \sim 400$, $\eta = 0.95$, and $Q_i \sim 10^8$, from Ref. [29], we obtain $\beta = 34$ THz and $\kappa_{1i}/2\pi = c/(\lambda Q_i) = 4.7$ MHz, respectively. Based on Eq. (16), we can numerically calculate the sensitivity factor S through the power transmission spectra to show the differences in three possible configurations (a single cavity, two indirectly coupled cavities, and a $\mathcal{PT}$-assisted three-cavity array). Figure 5 presents the sensitivity factor S (or the so-called transmission slope) as a function of the frequency detuning Δ for these three configurations. Compared with both a single cavity and two indirectly coupled cavities, clearly, the sensitivity is enhanced in the $\mathcal{PT}$-assisted three-cavity array.

In order to further verify the roles of the propagating phase factor θ and the $\mathcal{PT}$-symmetric structure, the maximum value of the sensitivity $S_{\max}$ versus θ with and without the $\mathcal{PT}$-symmetric structure is depicted in Fig. 6. As shown in Fig. 6, the $\mathcal{PT}$-assisted three-cavity array (see the solid blue line) provides an enhancement of more than three orders of magnitude in the sensitivity compared with the configuration of two indirectly coupled cavities without the assistance of the $\mathcal{PT}$-symmetric unit (see the dashed red line) when $\theta = n\pi + 0.19\pi$ (n is an integral number). From Fig. 6, the detection sensitivity dT/dn_s approaches 4×10^9 when the above-mentioned parameters $\beta = 34$ THz, $\kappa_{1i}/2\pi = 4.7$ MHz, and $\theta = n\pi + 0.19\pi$ are chosen, which means that the transmission rate will deviate by 0.4 even when n_s changes by only 10^{-10}. This is 10^2 times better than currently achievable with microresonators [29].

Figure 7 shows the dependence of the maximum value of the sensitivity $S_{\max}$ on the coupling strength J between loss cavity 2 and gain cavity 3. As shown, when J increases, first $S_{\max}$ increases slowly from a very small value, and then $S_{\max}$ increases very sharply, reaching a very high value. With a further increase in J, $S_{\max}$ drops sharply to a small value. From what has been analyzed above, we can reach the conclusion that, with properly choice of J, a significantly enhanced sensitivity ($S_{\max} \sim 10^6$, $dT/dn_s \sim 10^{12}$) can be

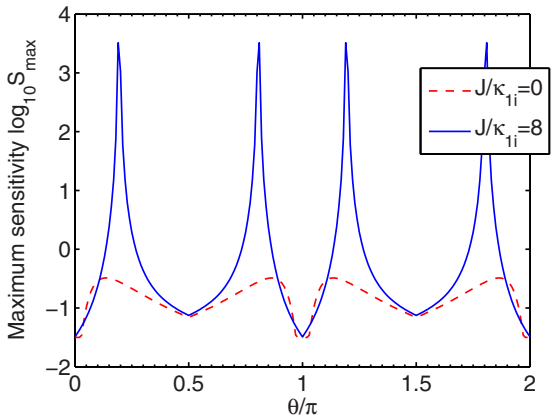

FIG. 6. Maximum sensitivity $S_{\max}$ versus propagating phase factor θ/π with the assisted $\mathcal{PT}$-symmetric structure (solid blue line; $J/\kappa_{1i} = 8$) and without the $\mathcal{PT}$-symmetric structure, i.e., in two indirectly coupled cavities (dashed red line; $J/\kappa_{1i} = 0$). Other system parameters for the simulation are chosen as $\kappa_{2e} = \kappa_{1e} = 20\kappa_{1i}$, $\kappa_{2i} = \kappa_{1i}$, and $\kappa_3 = -21\kappa_{1i}$, respectively.

realized in the $\mathcal{PT}$-assisted three-cavity array. In this situation, the best sensitivity is more than 10^5 higher than that of two indirectly coupled lossy cavities without assisting $\mathcal{PT}$ symmetry [29].

Before ending this section, we present a brief discussion of the relations between the above-mentioned EPs in the $\mathcal{PT}$-symmetric unit and the Fano-like profile observable in the resonance spectra. It is well known and was picked up again recently that asymmetric Fano line shapes can be traced back to the existence of EPs in the resonance spectra [71,72]. Likewise, the present $\mathcal{PT}$-symmetric cavity dimer features a $\mathcal{PT}$-symmetry phase transition when the coupling parameter J passes through the EP, i.e., $J \simeq (\kappa_{2e} + \kappa_{2i})/4$. Here the effective loss rates including the pump gain (e.g., κ_{2e}, κ_{2i}, and κ_3) are kept constant and the EP is obtained by diagonalizing the coefficient matrix of Eqs. (1)–(3). From the given system parameters in Fig. 7 (also see Fig. 4), we can obtain the EP

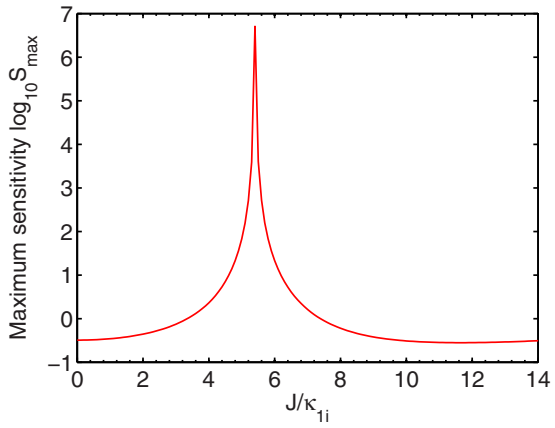

FIG. 7. Maximum sensitivity $S_{\max}$ versus intercavity coupling strength J/κ_{1i} for the $\mathcal{PT}$-assisted three-cavity array. Other system parameters for the simulation are chosen as $\kappa_{2e} = \kappa_{1e} = 20\kappa_{1i}$, $\kappa_{2i} = \kappa_{1i}$, $\kappa_3 = -21\kappa_{1i}$, and $\theta = \pi/8$, respectively.

value $J \simeq 5.3\kappa_{1i}$. In this context, it is easy to find from Fig. 7 that the sensitivity of the RI sensors is significantly enhanced in the vicinity of the EP. This confirms that the EP of the $\mathcal{PT}$-symmetric array plays a key role in the improvement of the RI sensors. Indeed, it has been shown in Ref. [66] that EPs are usable for drastic enhancement of the sensitivity of optical sensors based on the detection of splittings of resonant frequencies or energy levels. It should be pointed out that our RI sensor model for a single cavity coupled to a $\mathcal{PT}$-symmetric combination of two cavities via a waveguide based on detection of the transmitted power is also closely related to the approach proposed originally by Wiersig [66].

V. CONCLUSIONS

In summary, we have investigated the $\mathcal{PT}$-symmetry-induced evolution of sharp asymmetric line shapes in a three-cavity array side coupled to a channel waveguide. We discuss the difference in the generated line shapes in the output transmission spectra for three possible configurations (a single cavity, two indirectly coupled lossy cavities, and a $\mathcal{PT}$-assisted three-cavity array). It is shown that the three-cavity-array scheme based on $\mathcal{PT}$ symmetry can greatly enhance the sharp asymmetric Fano-like line shapes, which gives rise to faster changes in output transmission than the changes from both a single cavity and two indirectly coupled cavities. With the output transmission at a fixed wavelength that varies much more rapidly than it does in a single cavity and two indirectly coupled cavities, this $\mathcal{PT}$-assisted configuration results in a new type of high-sensitivity RI sensors for practical applications. For parameters based on microring resonators, the best sensitivity of RI sensors for the $\mathcal{PT}$-assisted three-cavity array is more than 10^5 higher than the configuration of two indirectly coupled cavities. Our obtained results can help us understand better the crossover between Fano resonances and $\mathcal{PT}$-symmetric theory. Also, the proposed scheme could provide a novel route toward line-shape engineering of Fano resonances in photonic structures by means of $\mathcal{PT}$-symmetric optical structures. We believe that the proposed structure is feasible in experimental realizations and deserves to be tested under the currently existing experimental conditions [28,50].

ACKNOWLEDGMENTS

We gratefully acknowledge the anonymous referees for their constructive comments and suggestions to improve the paper. We also acknowledge Xiao-Xue Yang and Xin-You Lü for useful advice and discussion of the manuscript preparation. J.L. and Y.W. were supported in part by the National Basic Research Program of China (973 Program) under Contract No. 2012CB922103 and the National Natural Science Foundation of China (NSFC) under Grants No. 11375067 and No. 11574104. R.Y. was supported by the NSFC under Grant No. 11505131 and the Youth Fund Project of Wuhan Institute of Technology under Grant No. Q201408. C.D. was supported by the NSFC under Grants No. 11447107 and No. U1504111, as well as the Doctoral Foundation of the Ministry of Education of China under Grant No. 20134103120005.

[1] K. J. Vahala, Optical microcavities, Nature (London) **424**, 839 (2003).

[2] F. Xia, L. Sekaric, and Y. A. Vlasov, Ultra-compact optical buffers on a silicon chip, Nat. Photon. **1**, 65 (2007).

[3] L. Zhang, M. Song, T. Wu, L. Zou, R. G. Beausoleil, and A. E. Willner, Embedded ring resonators for microphotonic applications, Opt. Lett. **33**, 1978 (2008).

[4] S. Fan, Manipulating light with photonic crystals, Physica B **394**, 221 (2007).

[5] S. Fan, Sharp asymmetric line shapes in side-coupled waveguide-cavity systems, Appl. Phys. Lett. **80**, 908 (2002).

[6] C. Y. Chao and L. J. Guo, Biochemical sensors based on polymer microrings with sharp asymmetrical resonance, Appl. Phys. Lett. **83**, 1527 (2003).

[7] A. M. Armani, R. P. Kulkarni, S. E. Fraser, R. C. Flagan, and K. J. Vahala, Label-free, single-molecule detection with optical microcavities, Science **317**, 783 (2007).

[8] J. Zhu, S. K. Ozdemir, Y. F. Xiao, L. Li, L. He, D. R. Chen, and L. Yang, On-chip single nanoparticle detection and sizing by mode splitting in an ultrahigh-Q microresonator, Nat. Photon. **4**, 46 (2010).

[9] Y. Xu, Y. Li, R. K. Lee, and A. Yariv, Scattering-theory analysis of waveguide-resonator coupling, Phys. Rev. E **62**, 7389 (2000).

[10] C. Manolatou, M. J. Khan, S. Fan, P. R. Villeneuve, H. A. Haus, and J. D. Joannopoulos, Coupling of modes analysis of resonant channel add-drop filters, IEEE J. Quantum Electron. **35**, 1322 (1999).

[11] S. Fan, P. R. Villeneuve, J. D. Joannopoulos, M. J. Khan, C. Manolatou, and H. A. Haus, Theoretical analysis of channel drop tunneling processes, Phys. Rev. B **59**, 15882 (1999).

[12] H. A. Haus and Y. Lai, Narrow-band distributed feedback reflector design, J. Lightwave Technol. **9**, 754 (1991).

[13] Q. Li, T. Wang, Y. Su, M. Yan, and M. Qiu, Coupled mode theory analysis of mode-splitting in coupled cavity system, Opt. Express **18**, 8367 (2010).

[14] D. D. Smith, H. Chang, K. A. Fuller, A. T. Rosenberger, and R. W. Boyd, Coupled-resonator-induced transparency, Phys. Rev. A **69**, 063804 (2004).

[15] A. Naweed, G. Farca, S. I. Shopova, and A. T. Rosenberger, Induced transparency and absorption in coupled whispering-gallery microresonators, Phys. Rev. A **71**, 043804 (2005).

[16] Y. Dumeige, S. Trebaol, and P. Feron, Intracavity coupled-active-resonator-induced dispersion, Phys. Rev. A **79**, 013832 (2009).

[17] J. K. Poon, L. Zhu, G. A. DeRose, and A. Yariv, Transmission and group delay of microring coupled-resonator optical waveguides, Opt. Lett. **31**, 456 (2006).

[18] K. Totsuka, N. Kobayashi, and M. Tomita, Slow Light in Coupled-Resonator-Induced Transparency, Phys. Rev. Lett. **98**, 213904 (2007).

[19] M. F. Yanik, W. Suh, Z. Wang, and S. Fan, Stopping Light in a Waveguide With An All-Optical Analog of Electromagnetically Induced Transparency, Phys. Rev. Lett. **93**, 233903 (2004).

[20] L. Maleki, A. B. Matsko, A. A. Savchenkov, and V. S. Ilchenko, Tunable delay line with interacting whispering-gallery-mode resonators, Opt. Lett. **29**, 626 (2004).

[21] Q. Xu, S. Sandhu, M. L. Povinelli, J. Shakya, S. Fan, and M. Lipson, Experimental Realization of An On-Chip All-Optical Analog To Electromagnetically Induced Transparency, Phys. Rev. Lett. **96**, 123901 (2006).

[22] Q. Xu, P. Dong, and M. Lipson, Breaking the delay-bandwidth limit in a photonic structure, Nat. Phys. **3**, 406 (2007).

[23] P. Chak, S. Pereira, and J. E. Sipe, Coupled-mode theory for periodic side-coupled microcavity and photonic crystal structures, Phys. Rev. B **73**, 035105 (2006).

[24] X. Yang, M. Yu, D.-L. Kwong, and C. W. Wong, All-Optical Analog to Electromagnetically Induced Transparency in Multiple Coupled Photonic Crystal Cavities, Phys. Rev. Lett. **102**, 173902 (2009).

[25] X. Yang, M. Yu, D. L. Kwong, and C. W. Wong, Coupled resonances in multiple silicon photonic crystal cavities in all-optical solid-state analogy to electromagnetically induced transparency, IEEE J. Sel. Top. Quantum Electron. **16**, 288 (2010).

[26] R. D. Kekatpure, E. S. Barnard, W. Cai, and M. L. Brongersma, Phase-Coupled Plasmon-Induced Transparency, Phys. Rev. Lett. **104**, 243902 (2010).

[27] J. Pan, S. Sandhu, Y. Huo, M. Povinelli, J. S. Harris, M. M. Fejer, and S. Fan, Experimental demonstration of an all-optical analog to the superradiance effect in an on-chip photonic crystal resonator system, Phys. Rev. B **81**, 041101 (2010).

[28] B.-B. Li, Y.-F. Xiao, C.-L. Zou, X.-F. Jiang, Y.-C. Liu, F.-W. Sun, Y. Li, and Q. Gong, Experimental controlling of Fano resonance in indirectly coupled whispering-gallery microresonators, Appl. Phys. Lett. **100**, 021108 (2012).

[29] Y. Xiao, V. Gaddam, and L. Yang, Coupled optical microcavities: An enhanced refractometric sensing configuration, Opt. Express **16**, 12538 (2008).

[30] Y. Xiao, M. Li, Y. Liu, Y. Li, X. Sun, and Q. Gong, Asymmetric Fano resonance analysis in indirectly coupled microresonators, Phys. Rev. A **82**, 065804 (2010).

[31] H. Lu, X. Liu, D. Mao, and G. Wang, Plasmonic nanosensor based on Fano resonance in waveguide-coupled resonators, Opt. Lett. **37**, 3780 (2012).

[32] C. M. Bender and S. Boettcher, Real Spectra in Non-Hermitian Hamiltonians Having $\mathcal{PT}$ Symmetry, Phys. Rev. Lett. **80**, 5243 (1998).

[33] C. M. Bender, Introduction to $\mathcal{PT}$-symmetric quantum theory, Contemp. Phys. **46**, 277 (2005).

[34] C. M. Bender, S. Boettcher, and P. N. Meisinger, $\mathcal{PT}$-symmetric quantum mechanics, J. Math. Phys. **40**, 2201 (1999).

[35] For a recent review, see C. M. Bender, Making sense of non-Hermitian Hamiltonians, Rep. Prog. Phys. **70**, 947 (2007); $\mathcal{PT}$ quantum mechanics—Recent results, AIP Conf. Proc. **1479**, 517 (2012).

[36] R. El-Ganainy, K. G. Makris, D. N. Christodoulides, and Z. H. Musslimani, Theory of coupled optical $\mathcal{PT}$-symmetric structures, Opt. Lett. **32**, 2632 (2007).

[37] S. Klaiman, U. Günther, and N. Moiseyev, Visualization of Branch Points in $\mathcal{PT}$-Symmetric Waveguides, Phys. Rev. Lett. **101**, 080402 (2008).

[38] K. G. Makris, R. El-Ganainy, D. N. Christodoulides, and Z. H. Musslimani, Beam Dynamics in $\mathcal{PT}$-Symmetric Optical Lattices, Phys. Rev. Lett. **100**, 103904 (2008).

[39] A. Guo, G. J. Salamo, D. Duchesne, R. Morandotti, M. Volatier-Ravat, V. Aimez, G. A. Siviloglou, and D. N. Christodoulides, Observation of $\mathcal{PT}$-Symmetry Breaking in Complex Optical Potentials, Phys. Rev. Lett. **103**, 093902 (2009).

[40] S. Longhi, Optical Realization of Relativistic Non-Hermitian Quantum Mechanics, Phys. Rev. Lett. **105**, 013903 (2010).

[41] C. E. Rüter, K. G. Makris, R. El-Ganainy, D. N. Christodoulides, M. Segev, and D. Kip, Observation of parity-time symmetry in optics, Nat. Phys. **6**, 192 (2010).
[42] S. Longhi, Bloch Oscillations in Complex Crystals With $\mathcal{PT}$ Symmetry, Phys. Rev. Lett. **103**, 123601 (2009).
[43] Y. D. Chong, L. Ge, and A. D. Stone, $\mathcal{PT}$-Symmetry Breaking and Laser-Absorber Modes in Optical Scattering Systems, Phys. Rev. Lett. **106**, 093902 (2011).
[44] A. Regensburger, C. Bersch, M.-A. Miri, G. Onishchukov, D. N. Christodoulides, and U. Peschel, Parity-time synthetic photonic lattices, Nature (London) **488**, 167 (2012).
[45] G. S. Agarwal and K. Qu, Spontaneous generation of photons in transmission of quantum fields in $\mathcal{PT}$-symmetric optical systems, Phys. Rev. A **85**, 031802(R) (2012).
[46] X. B. Luo, J. H. Huang, H. H. Zhong, X. Z. Qin, Q. T. Xie, Y. S. Kivshar, and C. H. Lee, Pseudo-Parity-Time Symmetry in Optical Systems, Phys. Rev. Lett. **110**, 243902 (2013).
[47] B. Peng, Ş. K. Özdemir, F. Lei, F. Monifi, M. Gianfreda, G. L. Long, S. Fan, F. Nori, C. M. Bender, and L. Yang, Parity-time-symmetric whispering-gallery microcavities, Nat. Phys. **10**, 394 (2014).
[48] L. Chang, X. Jiang, S. Hua, C. Yang, J. Wen, L. Jiang, G. Li, G. Wang, and M. Xiao, Parity-time symmetry and variable optical isolation in active-passive-coupled microresonators, Nat. Photon. **8**, 524 (2014).
[49] L. Feng, Z. J. Wong, R.-M. Ma, Y. Wang, and X. Zhang, Single-mode laser by parity-time symmetry breaking, Science **346**, 972 (2014).
[50] H. Hodaei, M. A. Miri, M. Heinrich, D. N. Christodoulides, and M. Khajavikhan, Parity-time-symmetric microring lasers, Science **346**, 975 (2014).
[51] H. Hodaei, M. A. Miri, A. U. Hassan, W. E. Hayenga, M. Heinrich, D. N. Christodoulides, and M. Khajavikhan, Parity-time-symmetric coupled microring lasers operating around an exceptional point, Opt. Lett. **40**, 4955 (2015).
[52] L. Ge, Parity-time symmetry in a flat-band system, Phys. Rev. A **92**, 052103 (2015).
[53] S. Longhi, $\mathcal{PT}$-symmetric laser absorber, Phys. Rev. A **82**, 031801 (2010).
[54] Z. Lin, H. Ramezani, T. Eichelkraut, T. Kottos, H. Cao, and D. N. Christodoulides, Unidirectional Invisibility Induced by $\mathcal{PT}$-Symmetric Periodic Structures, Phys. Rev. Lett. **106**, 213901 (2011).
[55] L. Ge, Y. D. Chong, and A. D. Stone, Conservation relations and anisotropic transmission resonances in one-dimensional $\mathcal{PT}$-symmetric photonic heterostructures, Phys. Rev. A **85**, 023802 (2012).
[56] M.-A. Miri, P. LiKamWa, and D. N. Christodoulides, Large area single-mode parity-time-symmetric laser amplifiers, Opt. Lett. **37**, 764 (2012).
[57] N. Bender, S. Factor, J. D. Bodyfelt, H. Ramezani, D. N. Christodoulides, F. M. Ellis, and T. Kottos, Observation of Asymmetric Transport in Structures With Active Nonlinearities, Phys. Rev. Lett. **110**, 234101 (2013).
[58] R. El-Ganainy, M. Khajavikhan, and L. Ge, Exceptional points and lasing self-termination in photonic molecules, Phys. Rev. A **90**, 013802 (2014).
[59] B. Peng, Ş. K. Özdemir, S. Rotter, H. Yilmaz, M. Liertzer, F. Monifi, C. M. Bender, F. Nori, and L. Yang, Loss-induced suppression and revival of lasing, Science **346**, 328 (2014).
[60] H. Jing, Ş. K. Özdemir, X.-Y. Lü, J. Zhang, L. Yang, and F. Nori, $\mathcal{PT}$-Symmetric Phonon Laser, Phys. Rev. Lett. **113**, 053604 (2014).
[61] S. Longhi and L. Feng, $\mathcal{PT}$-symmetric microring laser-absorber, Opt. Lett. **39**, 5026 (2014).
[62] X.-Y. Lü, H. Jing, J.-Y. Ma, and Y. Wu, $\mathcal{PT}$-Symmetry-Breaking Chaos in Optomechanics, Phys. Rev. Lett. **114**, 253601 (2015).
[63] H. Jing, Ş. K. Ödemir, Z. Geng, J. Zhang, X.-Y. Lü, B. Peng, L. Yang, and F. Nori, Optomechanically-induced transparency in parity-time-symmetric microresonators, Sci. Rep. **5**, 9663 (2015).
[64] J. Zhang, B. Peng, Ş. K. Özdemir, Y.-X. Liu, H. Jing, X.-Y. Lü, Y.-L. Liu, L. Yang, and F. Nori, Giant nonlinearity via breaking parity-time symmetry: A route to low-threshold phonon diodes, Phys. Rev. B **92**, 115407 (2015).
[65] Z.-P. Liu, J. Zhang, Ş. K. Özdemir, B. Peng, H. Jing, X.-Y. Lü, C.-W. Li, L. Yang, F. Nori, and Y.-X. Liu, Metrology with $\mathcal{PT}$-symmetric cavities: Enhanced sensitivity near the $\mathcal{PT}$-phase transition, arXiv:1510.05249.
[66] J. Wiersig, Enhancing The Sensitivity of Frequency and Energy Splitting Detection by Using Exceptional Points: Application to Microcavity Sensors for Single-Particle Detection, Phys. Rev. Lett. **112**, 203901 (2014).
[67] C. W. Gardiner, Driving a Quantum System With the Output Field From Another Driven Quantum System, Phys. Rev. Lett. **70**, 2269 (1993).
[68] H. J. Carmichael, Quantum Trajectory Theory for Cascaded Open Systems, Phys. Rev. Lett. **70**, 2273 (1993).
[69] J. D. Joannopoulos, S. G. Johnson, J. N. Winn, and R. D. Meade, *Photonic Crystals: Molding the Flow of Light*, 2nd ed. (Princeton University Press, Princeton, NJ, 2011).
[70] C. Wang and C. P. Search, Nonlinearly enhanced refractive index sensing in coupled optical microresonators, Opt. Lett. **39**, 26 (2014).
[71] A. I. Magunov, I. Rotter, and S. I. Strakhova, Fano resonances in the overlapping regime, Phys. Rev. B **68**, 245305 (2003).
[72] L. Schwarz, H. Cartarius, G. Wunner, W. D. Heiss, and J. Main, Fano resonances in scattering: An alternative perspective, Eur. Phys. J. D **69**, 196 (2015).